Redox Biology 45 (2021) 102052

Contents lists available at ScienceDirect

Redox Biology

journal homepage: www.elsevier.com/locate/redox

Acid ceramidase improves mitochondrial function and oxidative stress in Niemann-Pick type C disease by repressing STARD1 expression and mitochondrial cholesterol accumulation

Sandra Torres [a,b,1,2], Estel Solsona-Vilarrasa [a,b,1], Susana Nuñez [a,b], Nuria Matías [a,b], Naroa Insausti-Urkia [a,b], Fernanda Castro [a], Mireia Casasempere [c], Gemma Fabriás [c], Josefina Casas [c], Carlos Enrich [d,e], José C. Fernández-Checa [a,b,f,*,3], Carmen Garcia-Ruiz [a,b,f,**,3]

[a] Cell Death and Proliferation, Institute of Biomedical Research of Barcelona (IIBB), CSIC, Barcelona, Spain
[b] Liver Unit, Hospital Clinic I Provincial de Barcelona, IDIBAPS and CIBERehd, Barcelona, Spain
[c] Research Unit on BioActive Molecules (RUBAM), Departament de Química Orgànica Biològica, Institut d'Investigacions Químiques i Ambientals de Barcelona, Consejo Superior de Investigaciones Científicas (CSIC), Barcelona, Spain
[d] Departament de Biologia Cel·lular, Immunologia i Neurociències, Facultat de Medicina, Universitat de Barcelona, 08036, Barcelona, Spain
[e] Centre de Recerca Biomèdica CELLEX, Institut d'Investigacions Biomèdiques August Pi i Sunyer (IDIBAPS), 08036, Barcelona, Spain
[f] Research Center for ALPD, Keck School of Medicine, University of Southern California, Los Angeles, CA, USA

ARTICLE INFO

Keywords:
Cholesterol
Acid ceramiase
Mitochondrial function
Oxidative stress
NPC disease

ABSTRACT

Niemann-Pick type C (NPC) disease, a lysosomal storage disorder caused by defective NPC1/NPC2 function, results in the accumulation of cholesterol and glycosphingolipids in lysosomes of affected organs, such as liver and brain. Moreover, increase of mitochondrial cholesterol (mchol) content and impaired mitochondrial function and GSH depletion contribute to NPC disease. However, the underlying mechanism of mchol accumulation in NPC disease remains unknown. As STARD1 is crucial in intramitochondrial cholesterol trafficking and acid ceramidase (ACDase) has been shown to regulate STARD1, we explored the functional relationship between ACDase and STARD1 in NPC disease. Liver and brain of *Npc1*$^{-/-}$ mice presented a significant increase in mchol levels and STARD1 expression. U18666A, an amphiphilic sterol that inhibits lysosomal cholesterol efflux, increased mchol levels in hepatocytes from *Stard1*$^{f/f}$ mice but not *Stard1*$^{\Delta Hep}$ mice. We dissociate the induction of STARD1 expression from endoplasmic reticulum stress, and establish an inverse relationship between ACDase and STARD1 expression and LRH-1 levels. Hepatocytes from *Npc1*$^{+/+}$ mice treated with U18666A exhibited increased mchol accumulation, STARD1 upregulation and decreased ACDase expression, effects that were reversed by cholesterol extraction with 2-hydroxypropyl-β-cyclodextrin. Moreover, transfection of fibroblasts from NPC patients with ACDase, decreased STARD1 expression and mchol accumulation, resulting in increased mitochondrial GSH levels, improved mitochondrial functional performance, decreased oxidative stress and protected NPC fibroblasts against oxidative stress-mediated cell death. Our results demonstrate a cholesterol-dependent inverse relationship between ACDase and STARD1 and provide a novel approach to target the accumulation of cholesterol in mitochondria in NPC disease.

1. Introduction

Niemann-Pick type C (NPC) disease is an inherited and progressive lysosomal storage disorder that exhibits a wide array of symptoms, ranging from neurological deterioration, liver disease, splenomegaly and ultimately premature death [1]. NPC disease is caused by mutations

* Corresponding author. Cell Death and Proliferation, Institute of Biomedical Research of Barcelona (IIBB), CSIC, Barcelona, Spain.
** Corresponding author. Cell Death and Proliferation, Institute of Biomedical Research of Barcelona (IIBB), CSIC, Barcelona, Spain.
E-mail addresses: checa229@yahoo.com, josecarlos.fernandezcheca@iibb.csic.es (J.C. Fernández-Checa), cgrbam@iibb.csic.es (C. Garcia-Ruiz).
[1] These authors contributed equally to the work.
[2] Current address: Translation Heptology, Department of Internal Medicine I, Universitätsklinikum/Goethe-Universität, Frankfurt, Germany.
[3] Shared Senior authorship.

https://doi.org/10.1016/j.redox.2021.102052
Received 21 February 2021; Received in revised form 21 May 2021; Accepted 16 June 2021
Available online 19 June 2021

in the genes encoding NPC1/NPC2, two lysosomal resident proteins that work in tandem in the regulation of lysosomal cholesterol homeostasis [2,3]. Moreover, disease-causing mutations on quality control pathways involving the lysosome and endoplasmic reticulum (ER) have also been shown to contribute to NPC disease [4]. Defects in NPC1 account for up to 95% of NPC cases and given its role in lysosomal cholesterol egress, the primary biochemical feature of NPC disease is reflected in the lysosomal accumulation of unesterified cholesterol in brain and liver [1,2,5]. Besides cholesterol, lysosomal accumulation of glycosphingolipids is an additional characteristic feature of NPC disease [2,6–8], and the prevention of this event is the basis of miglustat, an EMA-approved therapy for patients with NPC disease.

In addition to lysosomes, cholesterol accumulation has also been reported in mitochondria of affected organs from *Npc1*$^{-/-}$ mice [9,10], a murine model which reproduces many of the pathological features of the human disease. Mitochondrial cholesterol accumulation has emerged as a critical factor in several diseases, including steatohepatitis, cancer or Alzheimer's disease, due in part to the regulation of mitochondrial function and limitation of mitochondrial antioxidant defenses [10–16]. In particular, mitochondrial cholesterol accumulation is known to decrease mitochondrial GSH (mGSH) stores by impairing cytosolic GSH transport into mitochondria [12,13] and this outcome has been shown to determine mitochondrial dysfunction and oxidative stress in NPC disease [7]. Moreover, replenishment of mGSH levels improved mitochondrial function in cerebellum, abrogated oxidative stress and extended the median and maximal life span of *Npc1*$^{-/-}$ mice [7]. Therefore, given the key role of cholesterol in regulating mGSH transport and associated consequences, understanding the molecular mechanisms involved in the trafficking of cholesterol to mitochondria may be of relevance in NPC disease. The trafficking of mitochondrial cholesterol is not well understood and involves different intracellular sources and different molecular players [17–19]. STARD3 (also known as MLN64) is thought to transfer cholesterol from endosomes to the mitochondrial outer membrane, and its overexpression has been shown to increase mitochondrial cholesterol levels in NPC cells [20]. However, targeted mutation of the MLN64 STAR domain results in modest alterations in cellular sterol metabolism [21]. On the other hand, STARD1, the founder member of the STAR family, plays a crucial role in the trafficking of cholesterol to mitochondrial inner membrane, where its availability is the rate-limiting step in steroidogenesis [17–19]. Moreover, mice with global STARD1 deletion develop lethal congenital lipoid hyperplasia and knockout mice die within 7–10 days after birth [22], indicating that other STAR members cannot replace STARD1 function. In addition, hepatocyte-specific STARD1 ablation prevents acetaminophen-mediated hepatic mitochondrial cholesterol accumulation without change in MLN64 expression [23]. Thus, while these findings indicate that STARD1 is key in the intramitochondrial trafficking of cholesterol, the mechanism of STARD1 regulation in NPC disease has not been previously explored. As ER stress and acid ceramidase (ACDase), a lysosomal enzyme that regulates ceramide homeostasis, have been shown to regulate STARD1 expression [23,24], our aim was to examine the contribution of ER stress and ACDase in STARD1 expression in NPC disease and its impact in regulating mitochondrial cholesterol levels. Our findings show a cholesterol-dependent inverse relationship between ACDase and STARD1 and provide evidence that ACDase-mediated downregulation of mitochondrial cholesterol content by repressing STARD1 improves mitochondrial performance and oxidative stress in fibroblasts from patients with NPC disease.

2. Results

2.1. Hepatic mitochondrial cholesterol accumulation and STARD1 upregulation in *Npc1*$^{-/-}$ mice

Accumulation of cholesterol in lysosomes caused by mutations in NPC1 is a hallmark of NPC disease [1–5]. Besides this event, accumulation of cholesterol in mitochondria of affected organs from *Npc1*$^{-/-}$ mice has also been initially reported but not well characterized [9,10]. Hence, before exploring potential mechanisms, we further analyzed hepatic mitochondrial cholesterol homeostasis in *Npc1*$^{-/-}$ mice. First, staining of liver sections with GST-PFO, which detects unesterified cholesterol levels in membranes [25], increased in liver from *Npc1*$^{-/-}$ mice compared to *Npc1*$^{+/+}$ mice, with similar findings seen with filipin staining (Fig. 1A). These results were further confirmed by HPLC analyses of liver homogenates and isolated mitochondria from *Npc1*$^{-/-}$ mice (Fig. 1B and C). Consistent with the increase in mitochondrial cholesterol loading, fluorescence anisotropy analysis of liver mitochondria from *Npc1*$^{-/-}$ mice labeled with the fluorescent probe DPH revealed an increase in mitochondrial membrane order compared to mitochondria from *Npc1*$^{+/+}$ mice (Fig. 1D). In addition, confocal microscopy analyses of primary mouse hepatocytes (PMH) from 6-week old *Npc1*$^{-/-}$ mice indicated increased filipin staining and colocalization with cytochrome c-labeled mitochondria (Fig. 1E and F), confirming that the increase in mitochondrial cholesterol levels occurs primarily in hepatocytes. As a potential mechanism accounting for the increase in mitochondrial cholesterol content, we examined the expression of STARD1, which plays a crucial role in the intramitochondrial cholesterol trafficking from the outer to inner mitochondrial membrane for metabolism [17–19,21–23]. Remarkably, STARD1 expression increased at the protein and mRNA level in liver of *Npc1*$^{-/-}$ mice (Fig. 1G; Supplementary Fig 1A). Moreover, expression of MLN64, an endosomal member of the STAR family involved in egress of cholesterol from endosomes to STARD1 in the mitochondrial outer membrane (18–20), increased in liver of *Npc1*$^{-/-}$ mice (Fig. 1G). These findings establish the increase in hepatic mitochondrial cholesterol levels that correlate with expression of STARD1.

2.2. Hepatocyte-specific STARD1 deletion prevents U18666A-induced mitochondrial cholesterol accumulation

Since hepatocyte-specific STARD1 ablation prevented hepatic mitochondrial cholesterol accumulation despite unchanged expression of MLN64 [23], we next focused on STARD1 and addressed its causal role in the accumulation of cholesterol to mitochondria, using an in vitro model of NPC1 using U18666A. U18666A is an amphiphilic cationic sterol that interferes with the trafficking of cholesterol and causes its increase in lysosomes, thus reproducing the NPC phenotype [26,27]. Incubation of HeLa cells with U18666A has been shown to cause the accumulation of cholesterol in mitochondria [28]. To test the role of STARD1 in mitochondrial cholesterol loading, we generated mice with STARD1 deletion in hepatocytes (*Stard1*$^{\Delta Hep}$) mice that had been recently characterized [23]. Hepatocytes from *Stard1*$^{f/f}$ mice incubated with U18666A exhibited increased cholesterol trafficking in mitochondria, as shown by confocal imaging analyses (Fig. 1H and I). However, U18666A-induced mitochondrial cholesterol accumulation was prevented in hepatocytes from *Stard1*$^{\Delta Hep}$ mice (Fig. 1H and I). These findings provide a causal role for STARD1 in the trafficking of cholesterol to mitochondria in NPC disease.

2.3. Fibroblasts from patients with NPC disease exhibit increased mitochondrial cholesterol levels and STARD1 expression

To validate the relevance of the preceding findings to human disease, we examined the homeostasis of mitochondrial cholesterol in fibroblasts from patients with NPC disease. In line with findings in liver, fibroblasts from patients with NPC disease (Npc$^{-/-}$) exhibited increased unesterified cholesterol levels determined by HPLC analysis in homogenate and isolated mitochondria compared to fibroblasts from control subjects (Npc$^{+/+}$) (Fig. 2A and B). Furthermore, confocal microscopy analyses of Npc$^{-/-}$ fibroblasts revealed mitochondrial unesterified cholesterol accumulation with respect to Npc$^{+/+}$ fibroblasts, as indicated by the colocalization of filipin and cytochrome *c* staining (Fig. 2C and D).

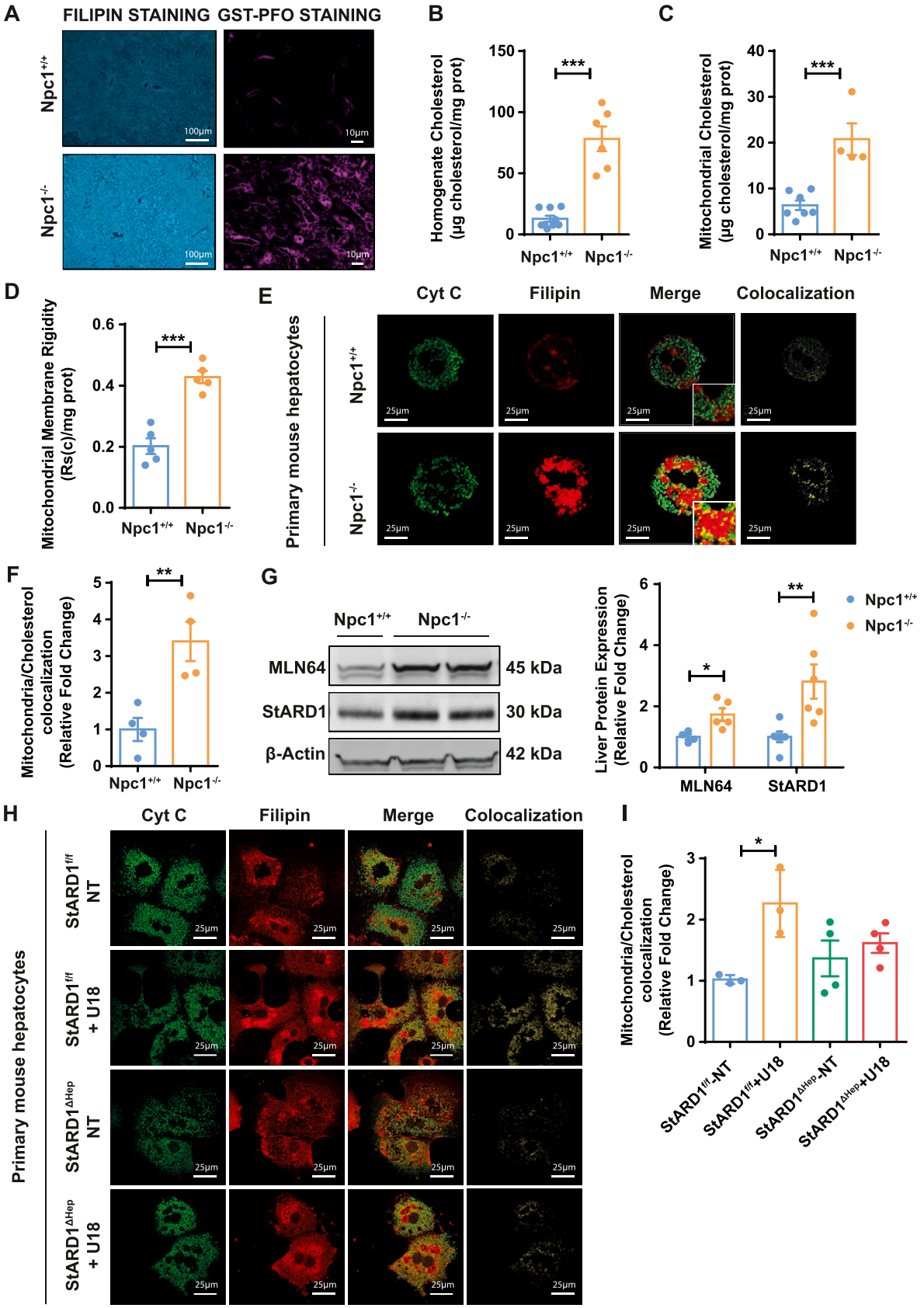

(caption on next page)

Fig. 1. Mitochondrial cholesterol trafficking and StARD1 expression in livers of Npc1$^{-/-}$ mice. Npc1$^{+/+}$ and Npc1$^{-/-}$ mice were sacrificed at 6 weeks of age to isolate mitochondria from liver. (A) Filipin and GST-PFO staining. (B) Homogenate and (C) mitochondrial cholesterol levels by HPLC analyses. (D) Mitochondrial membrane order measured by DPH fluorescence anisotropy. (E) Cytochrome *c* and Filipin co-staining for confocal microscopy analyses of Npc1$^{+/+}$ and Npc1$^{-/-}$ primary mouse hepatocytes. (F) Staining markers colocalization analysis using Image J software. (G) Western blot analyses and quantification of the mitochondrial cholesterol carriers StARD1 and MLN64 in liver of 6-weeks old Npc1$^{+/+}$ and Npc1$^{-/-}$ mice. Data are presented as means ± SEM (n > 4, Unpaired Student's t-test (two-tailed)). *p < 0.05, **p < 0.01, ***<0.001 vs. *Npc1*$^{+/+}$. (H-I) Primary mouse hepatocytes from StARD1f/f and StARD1ΔHep mice were treated with U18666A (U18, 2 μg/μl, 16 h) to determine (H) Cytochrome *c* and Filipin co-staining for confocal microscopy analyses and (I) Quantification of staining markers colocalization analysis using Image J software. Data are presented as means ± SEM (n > 3, One-way ANOVA followed byTukey's Multiple Comparison test). *p < 0.05 vs NT.

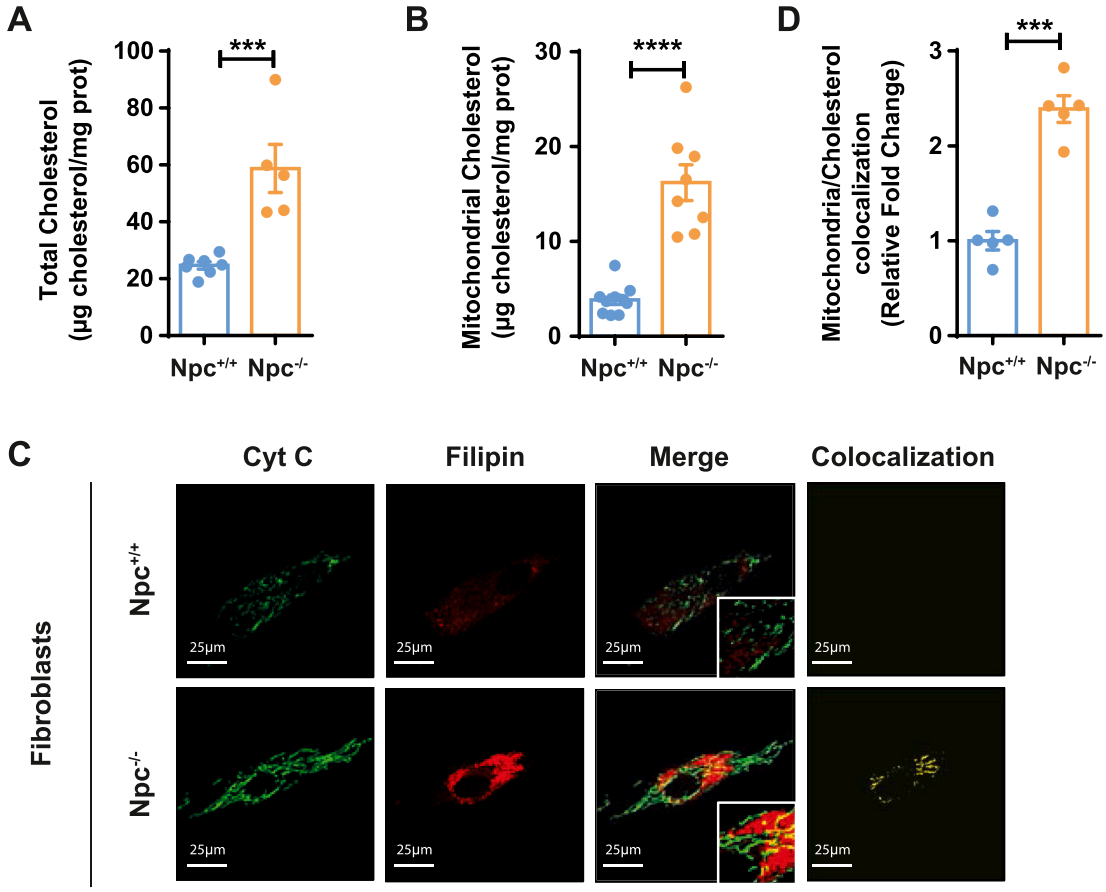

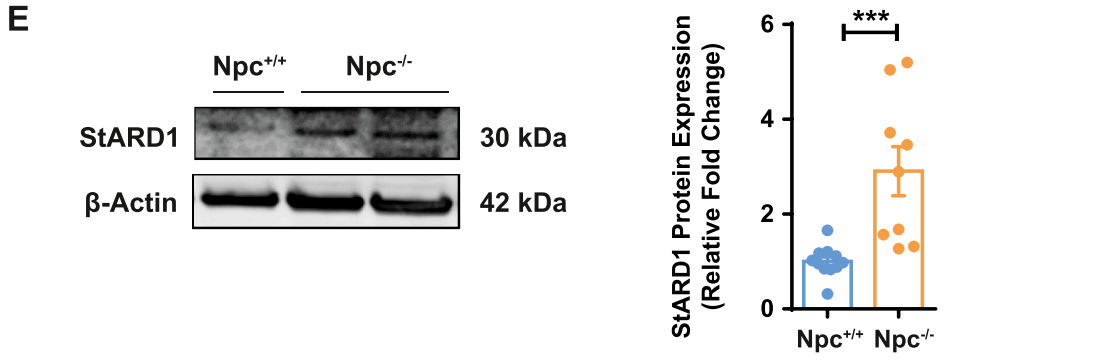

Fig. 2. Mitochondrial cholesterol trafficking and StARD1 expression in human skin fibroblasts from control subjects or patients with NPC disease. (A) Homogenate and (B) mitochondrial cholesterol levels by HPLC analyses. (C) Cytochrome *c* and Filipin co-staining for confocal microscopy analyses. (D) Staining markers colocalization analysis using Image J software. (E) Western blot analyses and quantification of the mitochondrial cholesterol carrier StARD1. Data are presented as means ± SEM (n > 5, Unpaired Student's t-test (two-tailed)). **p < 0.01, ***p < 0.001, ****p < 0.0001 vs. *Npc1*$^{+/+}$.

Furthermore, consistent with the enrichment in cholesterol, fluorescence anisotropy of mitochondria from Npc$^{-/-}$ fibroblasts labeled with DPH revealed increased order parameter (not shown). Moreover, STARD1 increased at the mRNA and protein levels in Npc$^{-/-}$ fibroblasts from patients with NPC disease compared to control Npc$^{+/+}$ fibroblasts (Fig. 2E; Supplementary Fig 1B). Thus, these findings confirm the

outcome observed in liver from *Npc1*$^{-/-}$ mice and reveal the mitochondrial cholesterol accumulation in human NPC disease.

2.4. Livers from *Npc1*$^{-/-}$ mice and fibroblasts from NPC patients exhibit decreased ACDase expression without evidence of ER stress

Given the relevance of STARD1 in the trafficking of cholesterol to mitochondrial inner membrane [22,23], we next examined potential mechanisms involved in the upregulation of STARD1 in NPC disease. ER stress has been shown to stimulate the transcriptional upregulation of STARD1 independently of SREBP activation [23,29], and hence we analyzed the expression of ER stress markers in liver from *Npc1*$^{-/-}$ mice and Npc$^{-/-}$ fibroblasts from patients with NPC disease. While tunicamycin induced markers of ER stress (BIP, PDI and CHOP) in control Npc$^{+/+}$ fibroblasts (Supplemetary Figure 2), the levels of ER stress markers BIP, PDI, CHOP, p-EIF2α and s-XBP1 in liver fractions from *Npc1*$^{-/-}$ mice or Npc$^{-/-}$ fibroblasts from patients with NPC disease were similar to those seen in *Npc1*$^{+/+}$ mice or control Npc$^{+/+}$ fibroblasts (Fig. 3A). These findings are in line with previous reports indicating that ER stress appears to play a minor role in lysosomal storage disorders, including NPC disease [30]. Given this outcome, we searched for alternative mechanisms involved in STARD1 regulation. As STARD1 is also regulated by steroidogenic factor 1 (SF-1), a member of the nuclear receptor family, and ACDase has been shown to repress SF-1 and subsequently STARD1 upregulation [24], we next examined ACDase expression in livers from *Npc1*$^{-/-}$ mice and Npc$^{-/-}$ fibroblasts from patients with NPC disease. Interestingly, the expression of ACDase decreased in liver and Npc$^{-/-}$ fibroblasts from NPC patients (Fig. 3B) and was further confirmed by confocal microscopy analyses in PMH from *Npc1*$^{-/-}$ mice and Npc$^{-/-}$ fibroblasts (Supplementary Fig 3A–D). Interestingly, the decreased level of ACDase protein was not due to impaired transcription, as the levels of mRNA in affected tissues of *Npc1*$^{-/-}$ mice or Npc fibroblasts were similar to control counterparts (Supplemetary Figure 4). These findings suggest that ACDase is regulated post-transcriptionally in NPC disease, consistent with the effect of MG132, a proteasome inhibitor, in increasing ACDase protein levels in human prostate cancer cells [31]. Moreover, as liver receptor homolog 1 (LRH-1), another member of the nuclear receptor family highly related to SF-1, regulates STARD1 [32], we examined its expression in NPC disease. As seen, LRH-1 levels increased in liver from *Npc1*$^{-/-}$ mice and in *Npc*$^{-/-}$ fibroblasts from NPC patients (Supplemetary Figure 5). Thus, these data revealed for the first time an inverse correlation between ACDase and STARD1 expression in NPC disease.

2.5. Mitochondrial cholesterol status and expression of STARD1 and ACDase in brain and cerebellum from *Npc1*$^{-/-}$ mice

We next examined the cholesterol homeostasis in brain homogenate from *Npc1*$^{-/-}$ mice. In contrast to liver, brain homogenate from *Npc1*$^{-/-}$ mice exhibited lower unesterified cholesterol levels compared to *Npc1*$^{+/+}$ mice, as revealed by filipin and GST-PFO staining or HPLC analyses (Supplementary Figure 6A, B), with similar findings observed in cerebellum from *Npc1*$^{-/-}$ mice (Supplementary Figure 7A, B). Since myelin is the major source of cholesterol in the brain, these findings are consistent with previous reports showing that in NPC disease cholesterol accumulates in most tissues but not the brain due to the extensive demyelination that occurs in this disease [33–36]. Quite interestingly, however, despite lack of increase of cholesterol levels in brain homogenate, isolated brain mitochondria exhibited increased mitochondrial cholesterol accumulation that resulted in increased mitochondrial membrane order (Supplementary Figure 6C, D), indicating the activation of a specific mechanism leading to increased mitochondrial cholesterol trafficking. Indeed, expression of STARD1 increased 4-fold in brain and cerebellum from *Npc1*$^{-/-}$ mice (Supplementary Figure 6E; Supplementary Figure 7C). In agreement with findings in liver, brain or cerebellum from *Npc1*$^{-/-}$ mice failed to exhibit signs of ER stress as revealed by the expression of BIP, PDI, CHOP, sXBP-1 and p-EIF2 (Supplementary Figure 6F; Supplementary Figure 7D). However, decreased levels of ACDase were observed in brain or cerebellum from *Npc1*$^{-/-}$ mice (Supplementary Figure 6G; Supplementary Figure 7E), in line with findings in liver. Overall these results confirm the accumulation of mitochondrial cholesterol in brain and cerebellum from *Npc1*$^{-/-}$ mice and further establish an inverse relationship between STARD1 and ACDase in these affected organs.

2.6. U18666A reproduces the inverse correlation between STARD and ACDase in *Npc1*$^{+/+}$ PMH

We next further characterized the relationship between STARD1 and ACDase. Since ACDase is a lysosomal enzyme, we first addressed whether the decrease in ACDase expression in NPC cells could be a consequence of the accumulation of cholesterol in lysosomes. Hence, we used the amphiphilic aminosteroid U186661, which antagonizes NPC1 and increases intracellular cholesterol accumulation. Confocal imaging analysis of PMH from *Npc1*$^{+/+}$ mice stained with filipin and Lamp2 revealed that U18666A significantly increased lysosomal cholesterol accumulation, reproducing the primary feature of NPC disease (Fig. 4A). In addition, U18666A also stimulated the accumulation of cholesterol in mitochondria, as seen by the colocalization of filipin and Cyt C staining of *Npc1*$^{+/+}$ PMH (Fig. 4B), in line with the findings seen in *Npc1*$^{-/-}$ PMH. Moreover, similar accumulation of mitochondrial cholesterol was observed in Npc$^{+/+}$ fibroblasts upon U18666A treatment (Fig. 5A and B). Interestingly, U18666A treatment significantly increased STARD1 in both PMH from *Npc1*$^{+/+}$ mice (Fig. 4C) and Npc$^{+/+}$ fibroblasts (Fig. 5C). In addition, in line with preceding findings in liver or brain tissues, U18666A treatment decreased the expression of ACDase in PMH from *Npc1*$^{+/+}$ mice (Fig. 4C) or control Npc$^{+/+}$ fibroblasts (Fig. 5C). Incubation of *Npc1*$^{+/+}$ PMH with U18666A failed to induce ER stress markers (Fig. 4D), consistent with findings in *Npc1*$^{-/-}$ PMH. Thus, these results provide evidence for a link between lysosomal cholesterol accumulation with ACDase repression and enhanced STARD1 expression.

2.7. 2-hydroxypropyl-β-cyclodextrin prevents U18666A-mediated ACDase downregulation and STARD1 upregulation

To further establish the role of cholesterol in the relationship between STARD1 and ACDase, we next examined the impact of 2-hydroxypropyl-β-cyclodextrin (HMβCD) in the expression of ACDase and STARD1 in response to U18666A. Treatment of Npc$^{+/+}$ fibroblasts from control patients or PMH from *Npc1*$^{+/+}$ mice with HMβCD prevented U18666A-induced cholesterol accumulation and trafficking to mitochondria in both cell types (Fig. 5A and B; Fig. 6A). Moreover, this outcome paralleled the ability of HMβCD to reverse the increase of STARD1 and the repression of ACDase induced by U18666A in control Npc$^{+/+}$ fibroblasts and PMH from *Npc1*$^{+/+}$ mice (Figs. 5C and 6B). PMH from *Npc1*$^{-/-}$ mice and Npc$^{-/-}$ fibroblasts from NPC patients exhibited the same changes induced by HMβCD regarding the reversed relationship between the expression levels of STARD1 and ACDase and the impact in mitochondrial cholesterol increase (Fig. 6C and D and Supplemetary Figure 8). These findings further establish a cholesterol-dependent relationship between STARD1 and ACDase.

2.8. ACDase overexpression in fibroblasts from NPC patients prevents STARD1 upregulation and mitochondrial cholesterol accumulation

To examine the cause-and-effect relationship between the decreased expression of ACDase and the induction of StARD1, we analyzed whether ACDase overexpression impact the regulation of STARD1. For this purpose, Npc$^{-/-}$ fibroblasts from NPC patients were transfected with cDNA encoding ACDase (MGC Human ASAH1 Sequence-Verified cDNA Accession: BC016481). Compared to transfection with scrambled

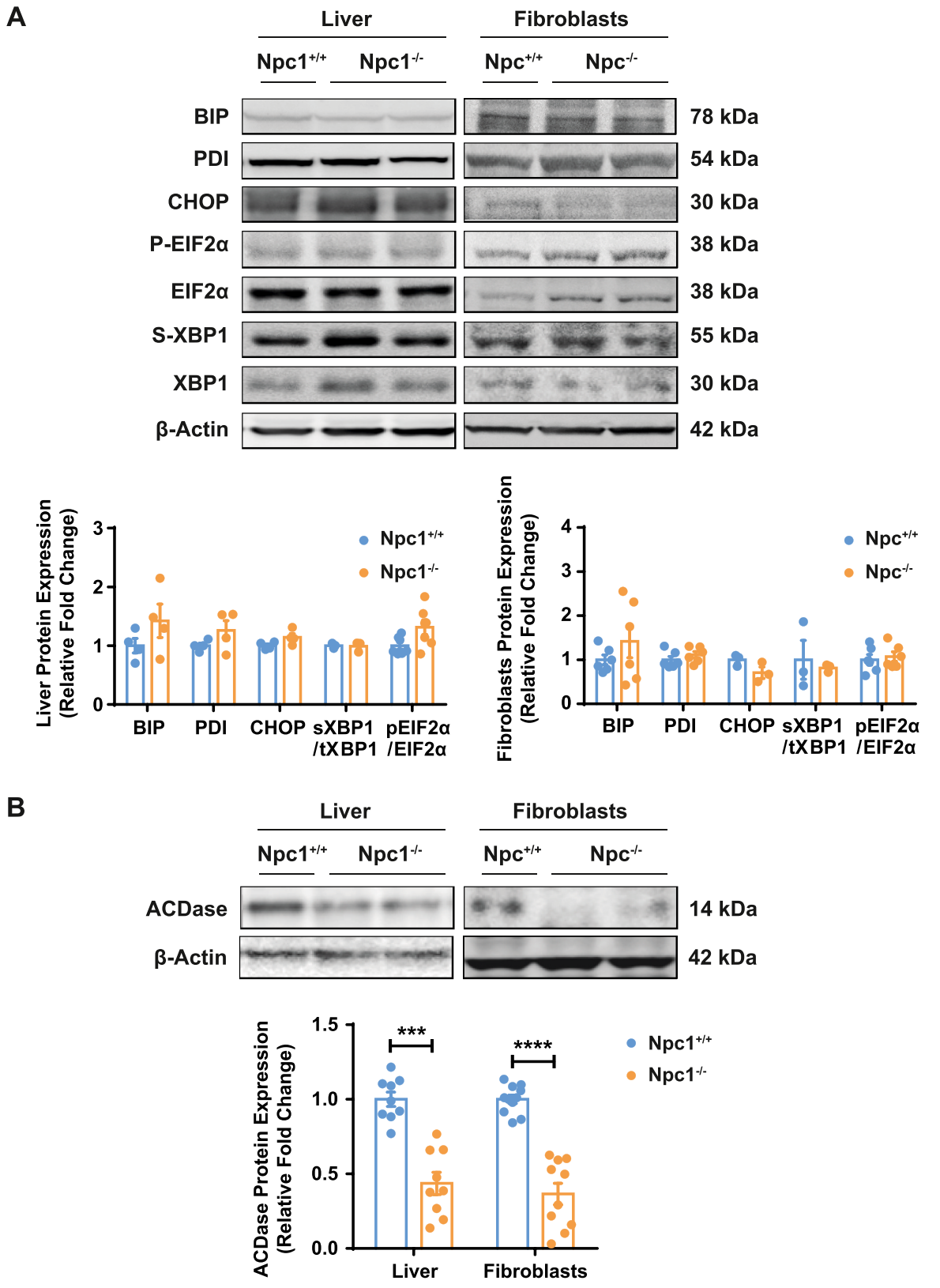

Fig. 3. ACDase and ER stress markers protein expression in livers from Npc1$^{-/-}$ mice and fibroblasts from NPC patients. A) ER stress markers and (B) ACDase protein expression analyzed by Western blot. Data are presented as means ± SEM (n > 3, Unpaired Student's t-test (two-tailed)). ***p < 0.001, ****p < 0.0001 vs. *Npc1*$^{+/+}$.

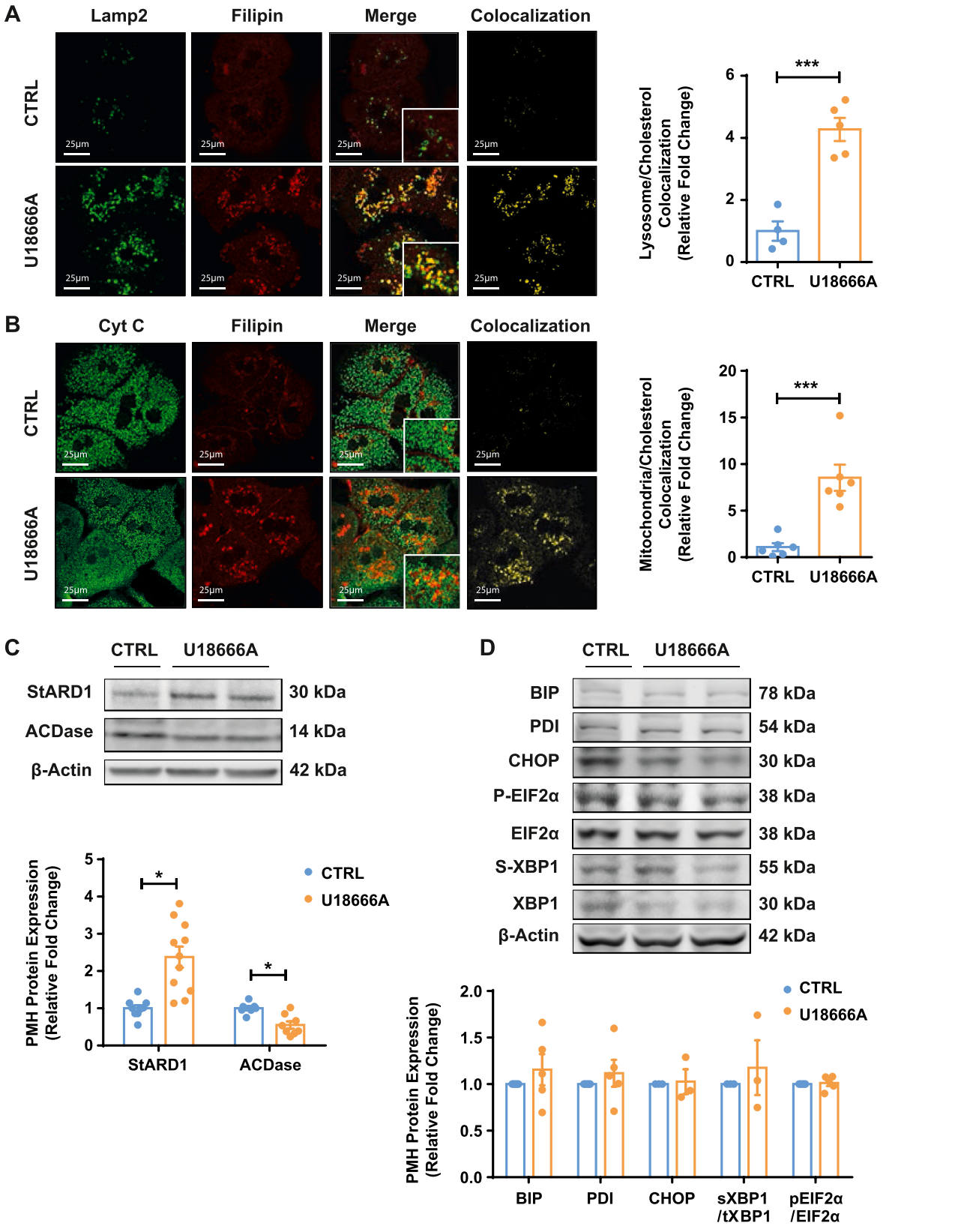

Fig. 4. Effects of U18666A treatment on liver mitochondrial cholesterol trafficking. Primary mouse hepatocytes from Npc1$^{+/+}$ were treated with U18666A (2 μg/μl, 16 h) to determine (A) Lysosomes and Filipin co-staining, (B) Mitochondria and Filipin co-staining for confocal microscopy analyses. Staining markers colocalization analysis using Image J software. (C) StARD1, ACDase and (D) ER stress markers protein expression analyzed by Western blot. Data are presented as means ± SEM (n > 5, Unpaired Student's t-test (two-tailed)). *p < 0.05, ***p < 0.001 vs. Control.

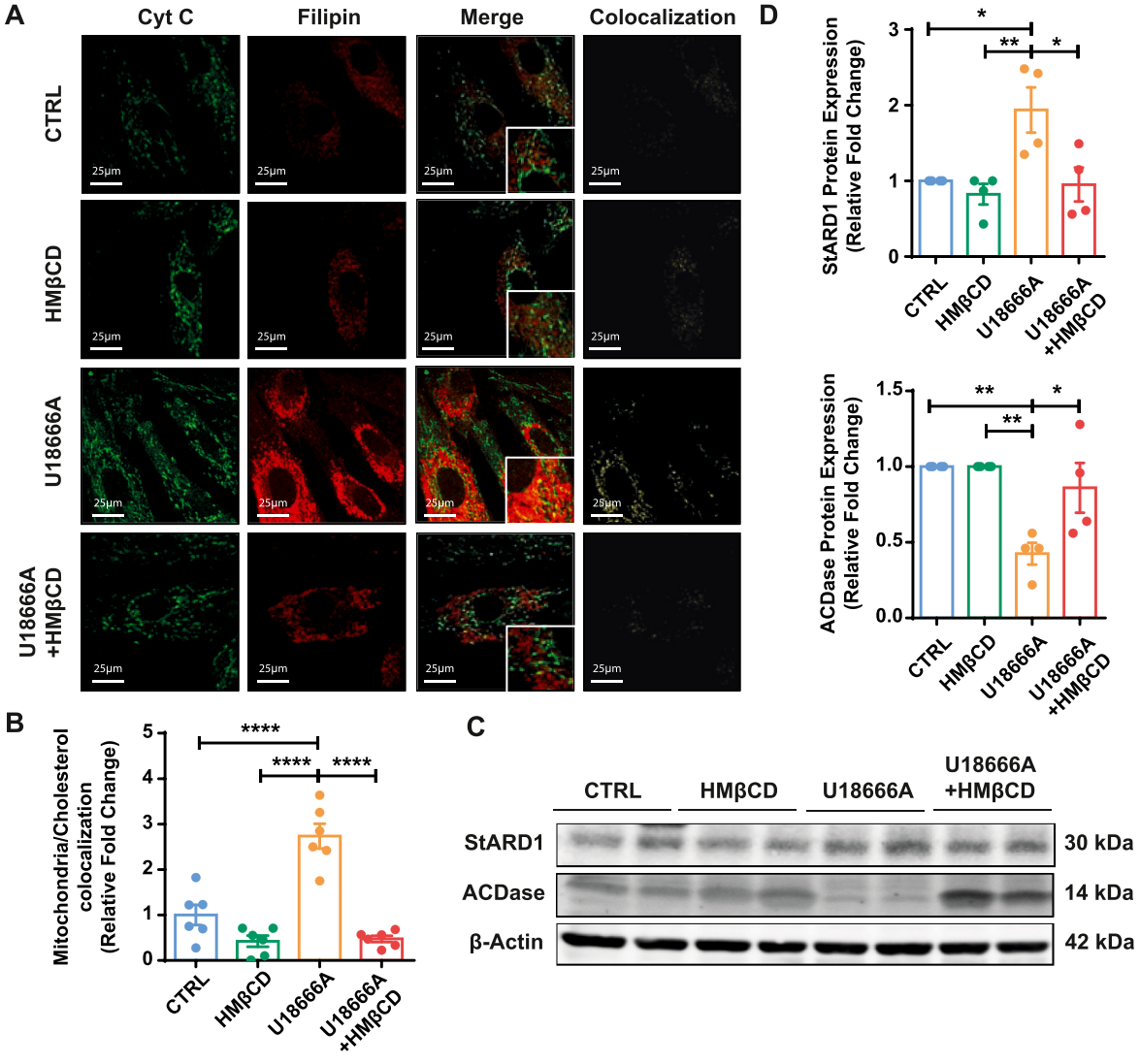

Fig. 5. Effects of U18666A on mitochondrial cholesterol trafficking and HMβCD modulation in human fibroblasts. Fibroblasts from control patients treated with U18666A (2 μg/μl, 16 h) were co-treated with HMβCD (2 mM, 16 h) to determine (A) Mitochondria and Filipin co-staining for confocal microscopy analyses. (B) Staining markers colocalization analysis using Image J software. (C) StARD1, and ACDase protein expression analyzed by Western blot. Data are presented as means ± SEM (n > 5, Unpaired Student's t-test (two-tailed)). *p < 0.05, **p < 0.01, ****p < 0.0001 vs. U18666A or control.

control GFP vector, ACDase transfection resulted in a 30-fold increase in ACDase expression (Fig. 7A), which translated in significantly higher ACDase protein levels (Fig. 7B). ACDase overexpression markedly decreased the expression of STARD1 in $Npc^{-/-}$ fibroblasts (Fig. 7B). Interestingly, given the role of LRH-1 in the transcriptional activation of STARD1, ACDase transfection repressed the expression of LRH-1 in $Npc^{-/-}$ fibroblasts from patients with NPC disease (Fig. 7C). To determine the impact of ACDase overexpression on the trafficking and accumulation of cholesterol in mitochondria, we performed confocal microscopy analyses of $Npc^{-/-}$ fibroblasts transfected with ACDase. $Npc^{-/-}$ fibroblasts from patients with NPC disease exhibited lower mitochondrial unesterified cholesterol levels as indicated by the colocalization of filipin with Cyt C staining, compared to scrambled control-GFP transfected fibroblasts (Fig. 7D). These findings indicate that ACDase expression represses STARD1 upregulation and decreases mitochondrial cholesterol accumulation in human NPC disease.

2.9. ACDase overexpression in fibroblasts from NPC patients increases mGSH, improves mitochondrial function and protects against oxidative stress and cell death

We next examined the functional impact of ACDase overexpression

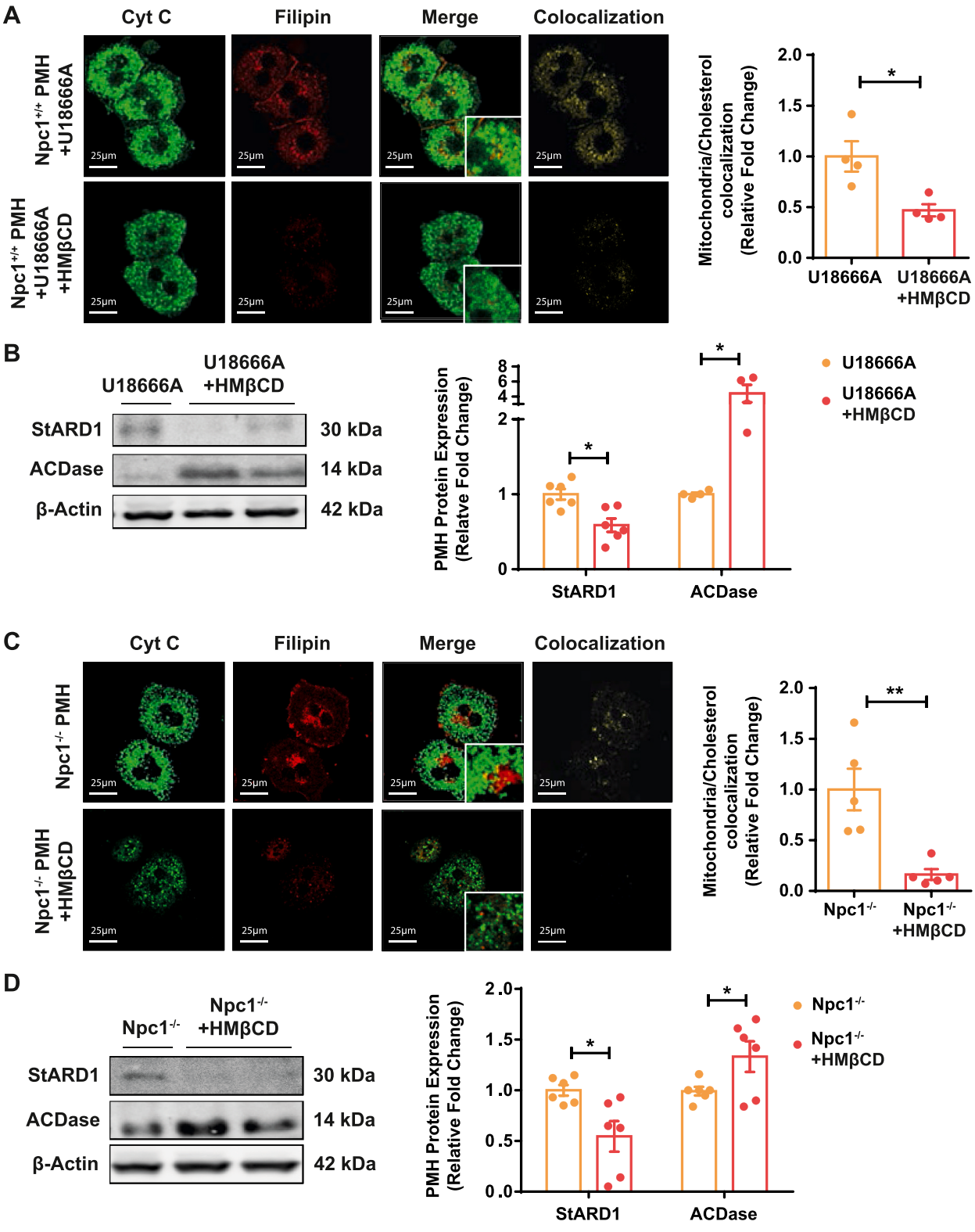

Fig. 6. Effects of HMβCD on hepatocytes from Npc1$^{+/+}$ mice treated with U18666A. Primary mouse hepatocytes from Npc1$^{+/+}$ treated with U18666A (2 μg/μl, 16 h) and primary mouse hepatocytes from Npc1$^{-/-}$ were co-treated with HMβCD (2 mM, 16 h) to determine (A–C) Mitochondria and Filipin co-staining for confocal microscopy analyses. Staining markers colocalization analysis using Image J software. (B–D) StARD1, and ACDase protein expression analyzed by Western blot. Data are presented as means ± SEM (n > 5, Unpaired Student's t-test (two-tailed)). *p < 0.05, **p < 0.01 vs. *U18666A or Npc1$^{-/-}$*.

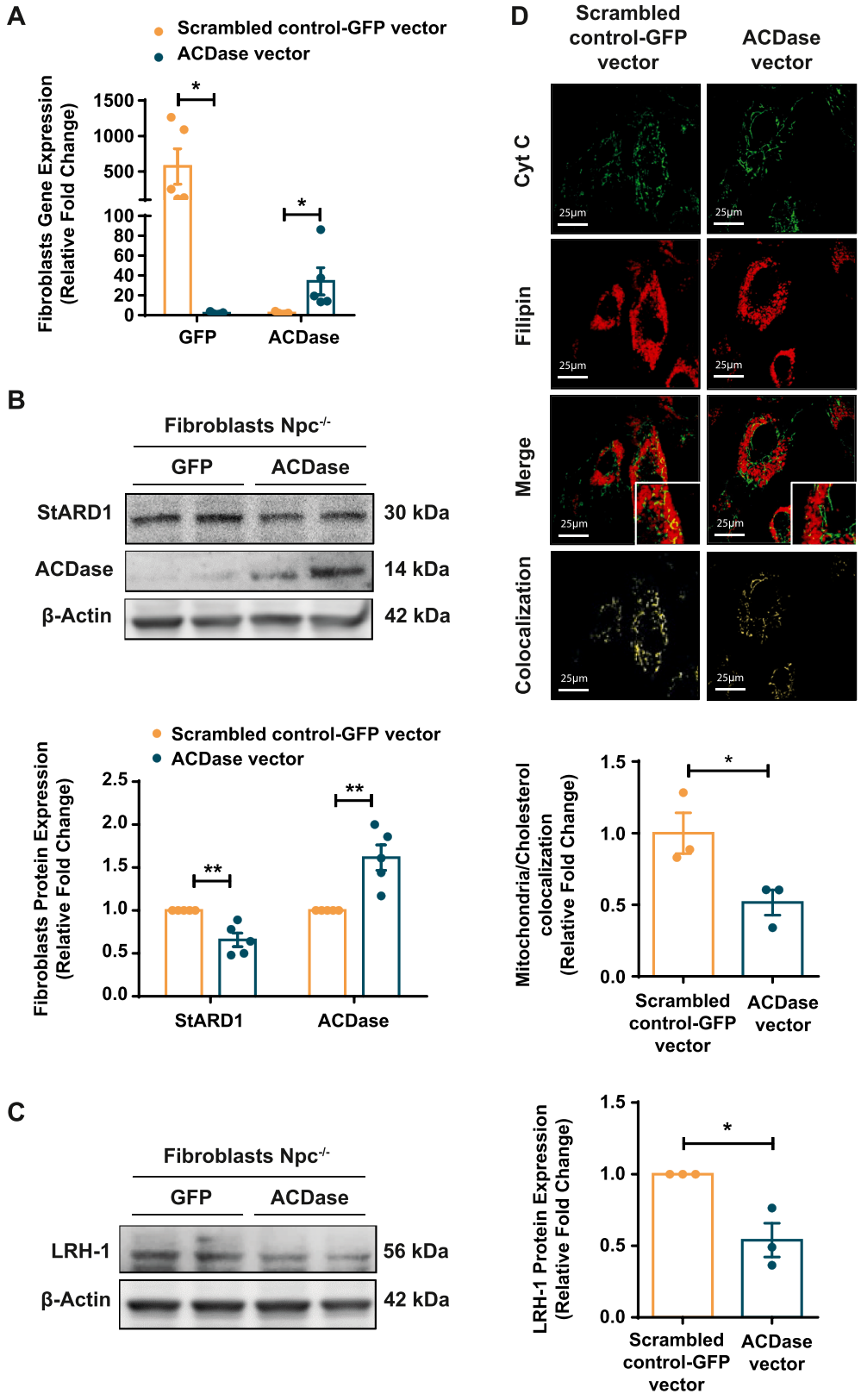

Fig. 7. ACDase overexpression in fibroblasts from NPC patients. Fibroblasts from NPC patients were transfected with a sobrexpression ACDase vector or the scrambled control-GFP vector to analyze (A) GFP and ACDase mRNA expression and (B) StARD1, and ACDase protein expression by Western blot. (C) LRH expression in fibroblasts from patients with NPC disease. Data are presented as means ± SEM (n = 3, Unpaired Student's t-test (two-tailed)). (D) Mitochondria and Filipin co-staining for confocal microscopy analyses. Staining markers colocalization analysis using Image J software. Data are presented as means ± SEM (n > 5, Unpaired Student's t-test (two-tailed)). *p < 0.05, **p < 0.01 vs. control GFP.

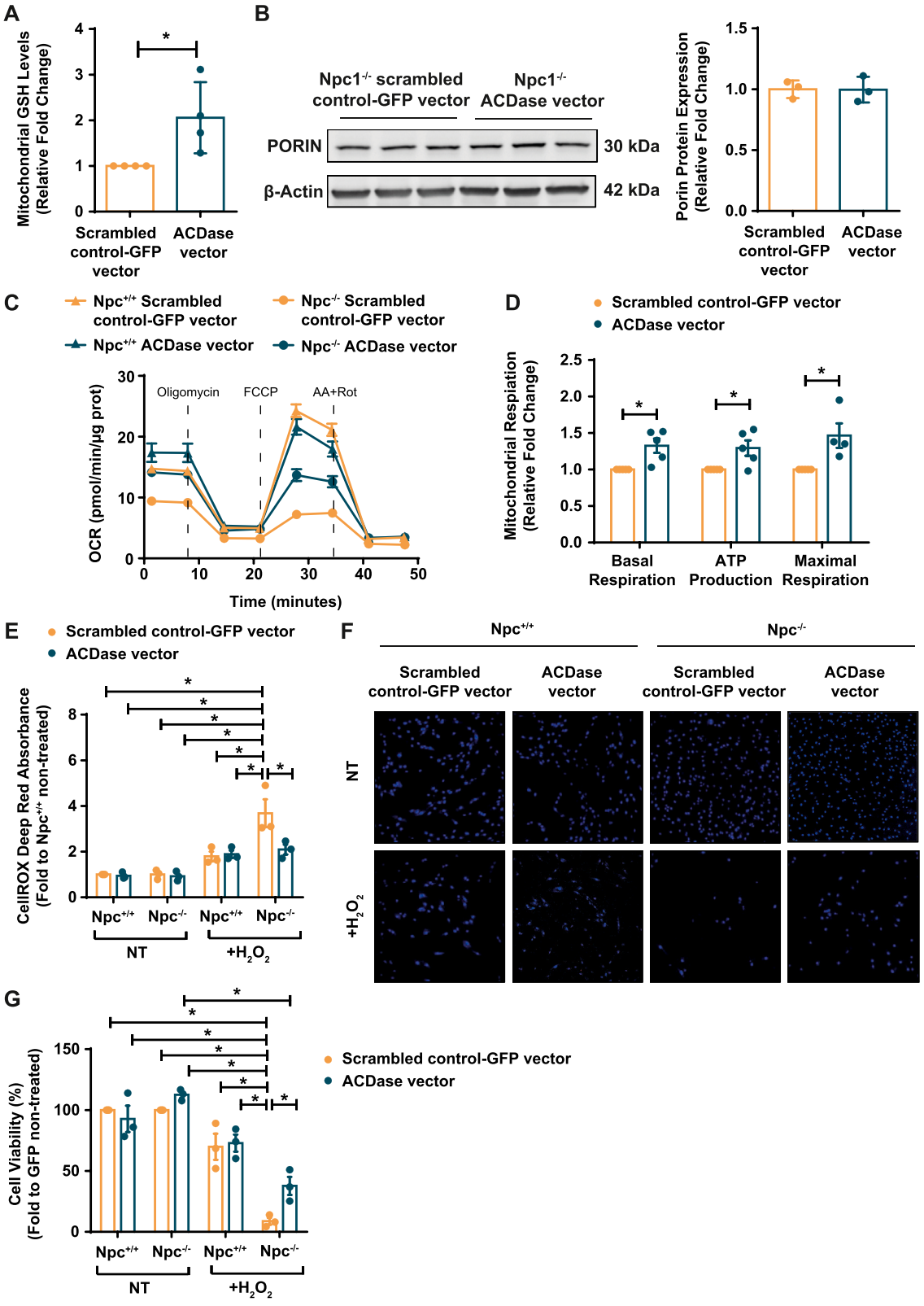

Fig. 8. ACDase overexpression improves mitochondrial function, and protects against oxidant cell death in fibroblasts from NPC patients. Fibroblasts from NPC patients were transfected with the ACDase vector or the scrambled control-GFP vector to analyze (A) mitochondrial GSH levels after cell fractionation by digitonin permeabilization, (B), porin levels to monitor mitochondrial mass, (C–D) oxygen consumption by Seahorse XF analyser and (E–G) ROS production and cell viability after treatment with H_2O_2 1 mM for 24 h followed by CellROX Deep Red absorbance and Höechst imaging respectively. Data are presented as means ± SEM (n = 3, Unpaired Student's t-test (two-tailed) or Two-way ANOVA test). *p < 0.05 vs NT or *Npc1*$^{+/+}$. (For interpretation of the references to colour in this figure legend, the reader is referred to the Web version of this article.)

in fibroblasts from NPC patients. Consistent with the ability of ACDase to decrease STARD1 expression and mitochondrial cholesterol accumulation (Fig. 7), $Npc^{-/-}$ fibroblasts from patients with NPC transfected with ACDase exhibited increased mGSH levels compared to fibroblasts transfected with control GFP vector (Fig. 8A). This outcome was not due to increased mitochondrial mass by ACDase overexpression as indicated by the unchanged levels of porin (Fig. 8B). Moreover, ACDase expression increased real-time oxygen consumption rates determined by an extracellular flux analyser compared to $Npc^{-/-}$ fibroblasts from NPC patients transfected with control GFP control vector (Fig. 8C), leading to enhanced rates of basal respiration, ATP production and maximal respiration (Fig. 8D). Furthermore, ACDase transfection also resulted in decreased oxidative stress in response to H_2O_2 challenge as revealed by lower CellROX Deep Red fluorescence compared to $Npc^{-/-}$ fibroblasts from NPC patients transfected with control GFP vector (Fig. 8E). In line with these observations, $Npc^{-/-}$ fibroblasts from NPC patients transfected with control GFP vector were sensitive to H_2O_2-induced oxidative cell death and this outcome was ameliorated by ACDase transfection (Fig. 8F and G), consistent with the replenishment of mGSH levels and attenuation of DCF fluorescence. Overall, these findings indicate that expression of ACDase has important functional consequences in fibroblasts from NPC patients.

3. Discussion

While the accumulation of cholesterol in lysosomes is a primary event in NPC disease and believed to promote disease progression, the disturbance of intracellular cholesterol trafficking is more extensive and affects other intracellular organelles. Here we further characterized the accumulation of cholesterol in mitochondria at the molecular level and provide evidence for a previously unrecognized relationship between ACDase and STARD1. Extending previous work focused on the role of mGSH depletion in NPC disease [7], we show increased mitochondrial cholesterol levels in the affected organs of *Npc1*$^{-/-}$ mice and in fibroblasts from NPC patients and its correlation with the expression of STARD1. While these members of the STAR family may work in tandem in the trafficking of cholesterol to mitochondria with MLN64 assisting in the mobilization of cholesterol from the ER to mitochondrial outer membrane [17–19], the action of STARD1 is crucial for the intramitochondrial cholesterol distribution to the inner membrane for metabolism. Although forced MLN64 overexpression results in mitochondrial cholesterol accumulation [20], global deletion of STARD1 in mice results in lethal congenital lipoid hyperplasia [22], arguing that in the absence of STARD1 other members of the family cannot compensate for the trafficking of cholesterol to mitochondrial inner membrane for metabolism and generation of steroid hormones. Moreover, hepatocyte-specific STARD1 deletion has been shown to prevent mitochondrial cholesterol accumulation in acetaminophen-mediated liver failure despite unchanged MLN64 expression [23]. In line with these findings, we provide evidence for a causal role of STARD1 in the accumulation of cholesterol in mitochondria, as this event is prevented in hepatocytes from *Stard1*$^{\Delta Hep}$ mice following exposure to U18666A, an amphiphilic sterol that reproduces the phenotype of NPC disease, including the accumulation of cholesterol in mitochondrial membranes [26–28].

Although ER stress has been shown to regulate STARD1 expression [23,29], the onset of ER stress is not a characteristic feature of NPC disease [30,37], and hence we searched for alternative mechanisms that could regulate STARD1 expression. We provide evidence for a previously unrecognized inverse relationship between ACDase and STARD1 expression in NPC disease. Built on previous findings in adrenocortical cells showing that ACDase antagonizes SF-1 and represses target genes, including STARD1 [24], we show that the increased expression of STARD1 correlates with lower levels of ACDase in liver and brain from *Npc1*$^{-/-}$ mice and in fibroblast from NPC patients. Importantly, we show that increased lysosomal cholesterol induced by U18666A reproduces the outcome seen in *Npc1*$^{-/-}$ mice in regards to the inverse relationship between ACDase and STARD1 expression. Consistent with this link between ACDase and STARD1, cholesterol extraction by HMβCD prevents U18666A-mediated decrease ACDase expression, resulting in subsequent reversal of U18666A-induced STARD1 upregulation. Interestingly, we observed a paralleled regulation between MLN64 and STARD1 expression in response to U18666A, which could reflect the fact that both carriers exhibit strong affinity for cholesterol determined by their STAR domain [17,18]. These findings underscore that the downregulation of ACDase appears to be a consequence of lysosomal cholesterol accumulation in NPC fibroblasts or PMH incubated with U18666A. Although further work will be required to understand the basis for the ACDase repression in NPC disease, it is conceivable that cholesterol accumulation in lysosomes may affect membrane physical properties, leading secondarily to the modulation of ACDase expression. Whether fluidization of lysosomes reverses the ACDase repression in NPC disease remains to be investigated. To further establish a specific relationship between ACDase with STARD1 expression, we overexpressed ACDase in fibroblasts from patients with NPC. This approach, which increased ACDase levels, resulted in the subsequent downregulation of STARD1. Of interest, while our findings suggest that STARD1 upregulation contributes to mitochondrial cholesterol accumulation, this event could be an additional consequence of impaired mitochondrial cholesterol metabolism. For instance, consistent with this possibility, reduced levels of CYP450scc (also known as CYP11A1) have been described in cerebellum of *Npc1*$^{-/-}$ mice, reflecting the disruption in neurosteroidogenesis and decreased levels of pregnenolone, the first steroid produced from mitochondrial cholesterol, in brain of *Npc1*$^{-/-}$ mice [38].

SF-1 (NR5A1) and LRH-1 (NR5A2) are two orphan members of the Ftz-F1 subfamily of nuclear receptors. While LRH-1 is expressed in tissues derived from endoderm, including intestine, liver and exocrine pancreas, as well as ovary, SF-1 is predominantly expressed in endocrine organs and brain [39]. As related members, both SF-1 and LRH-1 are known to regulate STARD1 [40–42]. Consistent with the tissue-specific expression of SF-1 and LRH-1, our findings reveal an increased expression of LRH-1 in liver from *Npc1*$^{-/-}$ mice and fibroblasts from NPC patients in line with the downregulation of ACDase, further establishing an inverse relationship between ACDase and LRH-1 that can account for the regulation of STARD1. In support for a causal role between LRH-1 and STARD1, previous reports in human granulosa tumor cells indicated that LRH-1 transactivates the STARD1 promoter through the −105 to −95 site, while targeted loss of LRH-1 in granulosa cells decreased STARD1 mRNA levels and progesterone production in transgenic mice in response to human chorionic gonadotrophin, causing a failure to ovulate [43,44]. Similar to the ability of ACDase to preserve mitochondrial performance despite lysosomal cholesterol storage, recent findings linked lysosomal and mitochondrial dysfunction in NPC disease to mTORC1 hyperactivation [45]. Interestingly, genetic and pharmacological inhibition of mTORC1 improved mitochondrial function without correcting lysosomal cholesterol accumulation [45]. These findings suggest that the defects in mitochondrial cholesterol homeostasis and function in NPC disease can be normalized independently of lysosomal cholesterol loading.

An interesting point that deserves further consideration is the relationship between the basal levels of ACDase and its enzymatic product sphingosine in NPC disease. Sphingosine is one of the glycosphingolipids whose levels increased in NPC disease [7,46]. As ACDase catalyzes the deacylation of ceramide to sphingosine, its lower expression would not account of the observed higher sphingosine levels in NPC disease. How can we reconcile increased sphingosine level with lower ACDase expression? Although the status of other CDases in NPC disease remains to be investigated, recent findings have reported lower expression of sphingosine kinase 1 in NPC disease [47]. As sphingosine is the substrate of sphingosine kinase 1, its downregulation may contribute to the higher levels of sphingosine in NPC disease.

Overall, the present study analyzed the molecular players that contribute to the mitochondrial cholesterol accumulation in NPC disease, and revealed a key link between ACDase and STARD1 in this event. At the functional level, we show that the reexpression of ACDase in fibroblasts from patients with NPC disease lowers STARD1 expression and causes a decrease in mitochondrial cholesterol accumulation, which in turn results in replenishment of mGSH levels, improvement of mitochondrial routine performance, and decrease in ROS generation and protection against oxidative stress-dependent cell death. Thus, these findings imply that ACDase emerges as a novel opportunity for treatment to prevent mitochondrial cholesterol loading and its known consequences on mitochondrial function and antioxidant defense, which are of potential relevance in NPC disease.

4. Materials and methods

4.1. Study design

This is a prospective study with the aim to examine the putative mechanisms of mitochondrial cholesterol accumulation, which is an additional feature of NPC disease besides the well-recognized accumulation of cholesterol in endolysosomes. *Npc1*$^{-/-}$ mice was used as a model of NPC disease, which reproduces many of the pathological signs observed in patients, including hepatosplenomegaly, neurological defects, cerebellar functional alterations, leading to motor impairment and premature death. In addition, fibroblasts from patients with NPC disease were used to address the relevance of the findings with Npc1$^{-/-}$ mice. The study included the isolation of mitochondria from liver and brain as well as the culture of PMH from Npc1$^{-/-}$ mice and fibroblasts from NPC patients. Most measurements, including western blots, confocal analyses, H&E and biochemical analyses were performed in an open fashion. To gain statistical power sample size was calculated based on previous and comparable studies in which a similar sample size reached statistically significance. The number of individual mice and experiments with primary mouse hepatocytes or human fibroblasts from patients with NPC disease are indicated in Figure Legends.

4.2. *Npc1*$^{-/-}$ model and *Stard1* $^{\Delta Hep}$ mice

Npc1$^{-/-}$ mice (NPC1^{NIH}, BALB/cJ strain) were obtained from The Jackson Laboratories. At the time of weaning (21 days), mice were genetically identified by PCR using DNA prepared from tail-tips and following the genotyping protocols provided by the supplier, as described previously [7]. Liver-specific Stard1 knockout (*Stard1*$^{\Delta Hep}$) mice were created by crossing *Stard1*$^{f/f}$ mice, which were generated by the Cre-lox technology, with Alb-Cre mice and have been recently characterized [23]. *Stard1*$^{\Delta Hep}$ and *Stard1*$^{f/f}$ littermates were used in this study to isolated primary hepatocytes. All procedures involving animals and their care were approved by the Ethics Committee of the University of Barcelona (protocol number 371/18) and were conducted in accordance with institutional guidelines in compliance with national and international laws and policies.

4.3. Fibroblasts from patients with NPC disease

Fibroblasts from patients with NPC disease used have been previously described [7]. Briefly, cultured human skin fibroblasts from control individuals (HSF; GM5659D) and patients with NPC disease were a generous gift from Thierry Levade, Laboratoire de Biochimie Metabolique, Institut Federatif de Biologie (CHU Toulouse, France) or obtained from Coriell Institute for Medical Research (GM03123, NJ, USA) and were grown at 37 °C in 5% CO_2. DMEM (Gibco) culture medium was supplemented with 10% fetal bovine serum (FBS, Gibco, 10-270-106) and 10.000U/ml Penicillin-Streptomycin (Gibco, 15140-122).

4.4. Primary mouse hepatocytes isolation

PMH were isolated by collagenase perfusion at a flow rate of 7–9 ml/min and cultured at a density of 2 × 105 cells in 12-well plates coated with rat tail collagen. Hepatocytes were cultured in DMEM/F12 culture media (Gibco, 21331-020) supplemented with 10% FBS for the first 3 h post isolation, together with 10.000U/ml Penicillin-Streptomycin (Gibco, 15140-122), 200 mM L-Glutamine (Gibco, 25030-024), 7.5 mM D-Glucose (Sigma, G6152) and 150 mM Hepes pH 7.4 (Sigma). For subsequent treatments, FBS was replaced for 1 mM methionine (Sigma, M5308).

4.5. In vitro treatments

PMH from Npc1$^{+/+}$ and human Npc$^{+/+}$ control fibroblasts were treated with U18666A (2 μg/ml) or HMβCD (2 mM) for 16 h. In some other cases, PMH from Npc1$^{-/-}$ and Npc$^{-/-}$ fibroblast from NPC patients were treated with HMβCD as above for control PMH.

4.6. ACDase overexpression

Fibroblasts from NPC patients were transfected with cDNA to overexpress ACDase (ASAH1) (MGC Human ASAH1 Sequence-Verified cDNA Accession: BC016481 Clone ID: 3923451) commercially purchased from GE Dharmacon. Transfection. This was performed using Lipofectamine2000 (Invitrogen). Briefly, 250000 fibroblasts were incubated with the transfection mixtures containing 250 ng of the sobrexpression ACDase vector or the scrambled control-GFP vector. Cells were assayed 48 h after transfection for mRNA and protein levels.

4.7. Real time PCR

Total RNA was isolated from fibroblasts with Trizol reagent following original protocol from Trizol's Reagent (manufacter's protocol). Quantitative Reverse Transcription Polymerase Chain Reaction (qRT-PCR) was performed using the iScript One-Step RT-PCR Kit with SYBR Green (Bio-Rad, Hercules, CA) following the manufacturer's instructions. Each reaction was run in duplicate to determine the threshold (CT) for each mRNA, and the amount of each cDNA relative to the β-Actin endogenous control was determined using the 2-ΔΔCt method. The following primer sequences synthesized from Invitrogen were used:

Gene	Accession #	Forward primer (5′-3′)	Reverse primer (5′-3′)
GFP	L29345	CAGGAGCGCACCATCTTCTT	CTTGTGCCCCAGGATGTTG
ASAH1 (ACDase)	NM_177924.5	AGTTGCGTCGCCTTAGTCCT	TGCACCTCTGTACGTTGGTC
ACTB	NM_001101.5	TTGCCGACAGGATGCAGAA	GCCGATCCACACGGAGTACT

4.8. Recombinant GST-PFO probe

To assess an effective localization of cholesterol in membranes of liver, brain and liver tissues, we used a recombinant Perfringolysin O (PFO) fusioned with Glutathione-S-Transferase (GST-PFO). In tissues, PFO is able to track cholesterol of outer and inner membranes when these have more than 30% mol of cholesterol and the fusion with GST allows the detection by immunofluorescence techniques. The production of recombinant GST-PFO probe has been described in [48]. The sequence to design the plasmid was from NCBI database: DNA M36704, the gen of PFO in the Clostridium perfringens genome. Additionally, the signal peptide was eliminated from the PFO gen to enable the intracellular stance of the protein. The resulted sequence was synthesized into the plasmid pGEX 4T-1 (GenScript) between the BamHI and SmaI restriction sites. The plasmid was engineered to make a fusion protein with the GST tag. After bacterial production, and protein extraction and purification, the GST-PFO probe was dialyzed, concentrated, quantified and stored at −80 °C.

4.9. Filipin and GST-PFO staining

Cryopreserved liver, brain and cerebellum samples from were cut on a cryostat at 14 μm thin sections and placed on glass slides. Sections were brought to RT for 30 min, fixed in 4% paraformaldehyde for 20 min and washed with PBS. For Filipin staining tissues were incubated with 25 μg/mL Filipin (Sigma) over night at 4 °C protected from the light. After washing, slices were mounted with prolong antifade mountant (Dako). For GST-PFO staining, the sections were permeabilized with 0.2% Triton X-100 in blocking buffer (5% goat serum + 1% BSA in PBS) for 2 h in a dark-humid chamber. Then, slices were incubated 3 h with the probe GST-PFO (20 μg/ml) in 1% Goat Serum containing 0.05% Triton X-100 in PBS. After washing × 3 with PBS, samples were incubated O.N. at 4 °C with primary antibody Glutathione-STransferase (GST) (Santa Cruz). Secondary antibodies were diluted 1:200 in 1% Goat Serum containing 0.05% Triton X-100 in PBS and incubated for 90 min at RT with the mix of anti-mouse Alexa fluor-532 (for GST). After washing, slices were incubated 5 min in sudan black 0.1% in 70% EtOH to minimize autofluorescence and mounted with prolong antifade mountant (Dako). Images for all samples were taken with a Leica TCS SP5 laser scanning confocal system with a 633 oil immersion objective APO CS numerical aperture 1.4 equipped with a DMI6000 inverted microscope.

4.10. Mitochondria isolation

Mitochondrial fraction was isolated from liver and brain by Percoll density grandient centrifugation as described previously [7,23]. Mitochondrial purity and cross contamination with extramitochondrial compartments was performed, as described previously [10,14]. Contamination of mitochondrial fraction with ER, plasma membrane and early and late endosomes was excluded by analisis of GRP78, ATPaseα1, Rab5A, and Rab11, respectively, (Supplemetary Figure 9). Alternatively, PMH and fibroblasts were fractionated into cytosol and mitochondria by digitonin permeabilization as described previously [10]. Briefly, cells were fractionated into cytosol and mitochondria by selectively permeabilizing the plasma membrane with digitonin and subsequent centrifugation through an oil layer with 10% trichloroacetic acid (TCA) at the bottom. Aliquots of the total, cytosolic and mitochondrial fractions were kept on ice for determination of GSH levels by the recycling method as previously described [10].

4.11. Cholesterol measurements

Total cholesterol determination in homogenates (1 mg/ml) or mitochondrial extracts (2.3 mg/ml) was performed upon saponification with alcoholic KOH followed by water:hexane 1:2 extraction. Hexane phase was evaporated in a speed vacuum and used for cholesterol measurement. Unesterified cholesterol was determined from the same unsaponified samples and analyzed by HPLC using Bondapak C18 10 μm reversed-phase column (30 cm × 4 mm inner diameter; Waters, Cromatografia, S.A., Barcelona, Spain), and 2-propanol/acetonitrile/water (60:30:10) as mobile phase at a flow rate of 1 ml/min as described [26]. The amount of cholesterol was calculated from standard curves and the identity of the peaks was confirmed by spiking the sample with known standards.

4.12. Measurement of fluorescence anisotropy

Fluidity of mitochondrial membranes was evaluated by fluorescence anisotropy of mitochondria-bound dye DPH. DPH (20 mM in tetrahydrofuran) was first diluted 100 times with 10 mM Tris-HCl, 150 mM KCl, 1 mM EDTA, pH 7.4. Subsequently, DPH was injected into stirred mitochondrial suspensions (0.5 mg/ml) and the mixture was incubated for 30 min at 37 °C. Fluorescence polarization was measured in a Hitachi spectrofluorometer at wavelengths of 366 nm for excitation and 425 nm for emission. The results are expressed as anisotropy units (r), where $r = (I0/I90)/(I0+2I90)$. I0 and I90 represent the intensities of light when polarizers were in parallel or perpendicular orientation, respectively. Light scattering and intrinsic fluorescence were routinely corrected by subtracting the signal obtained from unlabeled samples and the fluorescence of the buffer plus label alone.

4.13. ROS generation and cell viability

For ROS production and cell viability assays, fibroblasts were treated with hydrogen peroxide (H_2O_2) 1 mM for 24 h. For ROS production analysis, cells were then incubated with the cell-permeable CellROX Deep Red reagent (5 μM) solution for 30 min at 37 °C in the dark, washed with PBS and evaluated by fluorescence spectroscopy using the Tecan Infinite® 200 PRO multi-mode microplate reading (640 nm for excitation and 665 nm for emission). The fluorescence was normalized by protein content, determined by BCA protein assay. The induction of ROS was calculated with respect to control samples. For cell viability analysis, cells were incubated with Höechst (10 μg/ml) solution for 20 min at 37 °C in dark, washed with PBS, fixed with formalin 10% and evaluated in a fluorescence microscope Leica TCS-SPE DM2500. Viability was calculated as the difference between the final number of cells and the cells present in the non-treated condition.

4.14. Western blot analysis

100 mg of liver were homogenized with a pestle homogenizer in 1 ml of homobuffer (70 mM saccharose, 220 mM mannitol, 2 mM Tris-HCl pH 7.4, 0,1 mM EDTA, 0.1% fatty acid free BSA) supplemented with protease and phosphatase inhibitors (Roche). Liver homogenates were diluted 4 times with RIPA lysis buffer (Sigma) with anti-proteases and anti-phosphatases. Cells were washed with PBS and lysed with ice-cold RIPA lysis buffer supplemented with protease and phosphatase inhibitors. Samples were incubated 15min at 4 °C, vortexed and spun down for 5min at 10000 rpm. All supernatants were collected and quantified for protein concentration using Quick-Bradford reagent (Bio-Rad) and 20–50 μg of protein were subjected to 4–12% SDS–polyacrylamide gel electrophoresis (SDS-PAGE) (Bio-Rad, XT-Criterion). Proteins were electrotransferred at 4 °C onto Hybond ECL nitrocellulose membranes (Amersham) and 5% BSA solution in TBS-Tween was used to block the membranes for 1 h at room temperature. Membranes were incubated overnight with the following primary antibodies: anti-PDI (Cell Signaling, 24465), anti-CHOP (Cell Signaling, 2895S), anti-Phospho eiF2A (Cell Signaling, 9721S), anti-eiF2A (Cell Signaling, 9722) and anti-StARD1 (Abcam, ab58013), anti-BIP (Stressgen, SPA826), anti-XBP1 (Santa Cruz, CS-8015) and anti-Mln64 (Santa Cruz SC-292868), ACDAse (Sigma, SAB3500293), LRH-1 (Santa Cruz, Cs-

393369) and anti-β-Actin HRP-conjugated (Sigma, A3854). Membranes were thoroughly washed with TBS-Tween and incubated for 45min with their respective HRP-conjugated secondary antibodies. Pierce ECL Western Blotting Substrate (Thermo Scientific) was used to develop the membranes. Images were digitally captured by LAS4000 (GE Healthcare) and optical density was analyzed with ImageJ software.

4.15. Immunofluorescence and laser confocal imaging

PMH were fixed for 15min with 3.7% paraformaldehyde and permeabilized for 5min with 0.2% saponin dissolved in 0.5% BSA-fatty acid free (FAF) in PBS commercial buffer. Cells were blocked with 1% BSA FAF for 15 min. Cytochrome *c* (Cytc) (BD Pharmigen, #556432) and Lamp2 (Abcam, #ab13524) primary antibodies were incubated overnight in BSA 1% followed by a secondary antibody for 1 h at room temperature in BSA 0.1%. Filipin (50 mg/ml, Sigma) was added during the secondary antibody incubation and the following steps were performed in the dark. Stained samples were embedded in fluoromont (Sigma) and digital images were taken in a Leica SP2 laser scanning confocal microscope equipped with UV excitation, an argon laser, a 633/1.32 OIL PH3 CS objective and a confocal pinhole set at 1 Airy unit. All the confocal images shown were single optical sections. Scale bar represents 25 μm. Percentage of cholesterol mass containing mitochondria was analyzed with the *Colocalization nBits nimages* plugin (Confocal Microscopy Unit, Facultad de Medicina, Universidad de Barcelona) in the Image J Software in 5 consecutive images of each experimental condition as described before [49]. This plug-in sofware highlights the colocalized points of two images of 32-bits, and returns the integrated densities of total green (higher than the threshold) and the green from colocalized points and total red (higher than the threshold) and red from colocalized points. Two points are considered as colocalized if their respective intensities are strictly higher than the threshold of their channels and if their ratio of intensity is strictly higher than the ratio setting value, which have been defined at 50%. Percentage of green colocalization with red or red colocalization with green is calculated as the ratio of green colocalized points divided by total green multiplied per 100 or as the ratio of red colocalized points divided by total red multiplied per 100, respectively.

4.16. Extracellular flux analyses

In vivo real-time mitochondrial respiration (OCR) was monitored with the Seahorse XFe24 Flux Analyser (Seahorse Bioscience) according to the manufacturer's instructions. Fibroblasts were seeded at 20000 fibroblasts/well density in 24-well plates and cultured overnight in DMEM culture media. For assessment of the real-time OCR, cells were incubated with unbuffered assay media (XF Media Base with 10 mM glucose, 1 mM L-glutamine and 1 mM sodium pyruvate) followed by a sequential injection of 2 μM oligomycin, 1 μM carbonyl cyanide-4-(trifluoromethoxy) phenylhydrazone and 1 μM antimycin A plus Rotenone. OCR measurements were normalized to μg of total protein following BCA protein assay.

4.17. Statistical analyses

Statistical analyses were performed using GraphPad Prism 6 (Graphpad Software Inc). Unpaired Student's t-test (two tailed) was performed between two groups and one or two-way ANOVA followed by Tukey's Multiple Comparison test were used for statistical comparisons between three or more groups, with $p < 0.05$ considered as significant (*$p < 0.05$, **$p < 0.01$, ***$p < 0.001$, ****$p < 0.0001$). The corresponding number of experiments is indicated in the figure legends. Data in graphs are shown as mean ± SEM.

Author contribution

Each author contributed to the planning, performance and analyses of the data. ST, ES-V, SN, NM, NI-U, FC performed most of the experiments with Npc1 null mice and human fibroblasts. MC, GF, JC and CE provided expertise, valuable suggestions and human fibroblasts. CGR and JCFC planned and design the study, participated in data analyses and discussions and wrote the manuscript with assistance from all authors.

Declaration of competing interest

The authors declare no competing financial interests.

Acknowledgements

We acknowledge the support from grants SAF2017-85877R, PID2019-111669RB-100 and PID2020-115055RB-I00 from Plan Nacional de I+D funded by the Agencia Estatal de Investigación (AEI) and the Fondo Europeo de Desarrollo Regional (FEDER) and from the CIBER-EHD; the center grant P50AA011999 Southern California Research Center for ALPD and Cirrhosis funded by NIAAA/NIH; as well as support from AGAUR of the Generalitat de Catalunya SGR-2017-1112, European Cooperation in Science & Technology (COST) ACTION CA17112 Prospective European Drug-Induced Liver Injury Network, the "ER stress-mitochondrial cholesterol axis in obesity-associated insulin resistance and comorbidities"-Ayudas FUNDACION BBVA and the Red Nacional 2018-102799-T de Enfermedades Metabólicas y Cáncer and the Project 201916/31 Contribution of mitochondrial oxysterol and bile acid metabolism to liver carcinogenesis 2019 by Fundació Marato TV3. E.S. V. was supported by a contract from the "Ministerio de Educación, Cultura y Deporte" (FPU15/04537) of the Spanish Government.

Appendix A. Supplementary data

Supplementary data to this article can be found online at https://doi.org/10.1016/j.redox.2021.102052.

References

[1] M.C. Patterson, et al., Recommendations for the diagnosis and management of Niemann-Pick disease type C: an update, Mol. Genet. Metabol. 106 (2012) 330–344.
[2] M.T. Vanier, Complex lipid trafficking in Niemann-Pick disease type C, J. Inherit. Metab. Dis. 38 (2015) 187–199.
[3] H.J. Kwon, et al., Structure of N-terminal domain of NPC1 reveals distinct subdomains for binding and transfer of cholesterol, Cell 137 (2009) 1213–1224.
[4] M.L. Schultz, K.L. Krus, A.P. Lieberman, Lysosome and endoplasmic reticulum quality control pathways in Niemann-Pick type C disease, Brain Res. 1649 (PtB) (2016) 181–188, https://doi.org/10.1016/j.brainres.2016.03.035.
[5] E.P. Beltroy, et al., Cholesterol accumulation and liver cell death in mice with Niemann-Pick type C disease, Hepatology 42 (2005) 886–893.
[6] M. Fan, et al., Identification of Niemann-Pick C1 disease biomarkers through sphingolipid profiling, J. Lipid Res. 54 (2013) 2800–2814.
[7] S. Torres, et al., Mitochondrial GSH replenishment as a potential therapeutic approach for Niemann Pick type C disease, Redox Biol (2017), https://doi.org/10.1016/j.redox.2016.11.010 [published online ahead of print.
[8] S. Torres, et al., Lysosomal and mitochondrial liaisons in niemann-pick disease, Front. Physiol. 8 (2017 Nov 30) 982, https://doi.org/10.3389/fphys.2017.00982.
[9] W. Yu, et al., Altered cholesterol metabolism in Niemann-Pick type C1 mouse brains affects mitochondrial function, J. Biol. Chem. 280 (12) (2005) 11731–11739.
[10] M. Marí, et al., Mitochondrial free cholesterol loading sensitizes to TNF- and Fas-mediated steatohepatitis, Cell Metabol. 4 (3) (2006) 185–198.
[11] F.R. Maxfield, I. Tabas, Role of cholesterol and lipid organization in disease, 2005, https://doi.org/10.1038/nature04399. Nature [published online ahead of print.
[12] S.-D. Ha, S. Park, C.Y. Han, M.L. Nguyen, S.O. Kim, Cellular adaptation to anthrax lethal toxin-induced mitochondrial cholesterol enrichment, hyperpolarization, and reactive oxygen species generation through downregulating MLN64 in macrophages, Mol. Cell Biol. 32 (23) (2012) 4846–4860.
[13] M. Marí, A. Morales, A. Colell, C. García-Ruiz, J.C. Fernández-Checa, Mitochondrial glutathione, a key survival antioxidant, Antioxidants Redox Signal. 11 (11) (2009) 2685–2700.

[14] A. Fernández, L. Llacuna, J.C. Fernández-Checa, A. Colell, Mitochondrial cholesterol loading exacerbates amyloid beta peptide-induced inflammation and neurotoxicity, J. Neurosci. Off. J. Soc. Neurosci. 29 (20) (2009) 6394–6405.
[15] E. Solsona-Vilarrasa, et al., Cholesterol enrichment in liver mitochondria impairs oxidative phosphorylation and disrupts the assembly of respiratory supercomplexes, Redox Biology 24 (2019) 101214. Jun.
[16] J. Montero, et al., Mitochondrial cholesterol contributes to chemotherapy resistance in hepatocellular carcinoma, Canc. Res. 68 (13) (2008) 5246–5256. Jul 1.
[17] Miller WL. Disorders in the initial steps of steroid hormone synthesis. J. Steroid Biochem. Mol. Biol. [published online ahead of print: March 2016]; doi:10.1016/j.jsbmb.2016.03.009.
[18] P. Elustondo, P. Martin, B. Karten, Mitochondrial cholesterol import, Biochim. Biophys. Acta Mol. Cell Biol. Lipids 1862 (1) (2017 Jan) 90–101.
[19] M. Charman, B.E. Kennedy, N. Osborne, B. Karten, MLN64 mediates egress of cholesterol from endosomes to mitochondria in the absence of functional Niemann-Pick Type C1 protein, J. Lipid Res. 51 (5) (2010) 1023–1034.
[20] E. Balboa, et al., MLN64 induces mitochondrial dysfunction associated with increased mitochondrial cholesterol content, Redox Biol 12 (2017) 274–284, https://doi.org/10.1016/j.redox.2017.02.024, 2017 Aug.
[21] T. Kishida, et al., Targeted mutation of the MLN64 START domain causes only modest alterations in cellular sterol metabolism, J. Biol. Chem. 279 (18) (2004) 19276–19285.
[22] K.M. Caron, et al., Targeted disruption of the mouse gene encoding steroidogenic acute regulatory protein provides insights into congenital lipoid adrenal hyperplasia, Proc. Natl. Acad. Sci. U.S.A. 94 (21) (1997) 11540–11545.
[23] S. Torres, et al., Endoplasmic reticulum stress-induced upregulation of STARD1 promotes acetaminophen-induced acute liver failure, Gastroenterology 157 (2) (2019) 552–568, https://doi.org/10.1053/j.gastro.2019.04.023. Aug.
[24] N.C. Lucki, et al., Acid ceramidase (ASAH1) represses steroidogenic factor 1-dependent gene transcription in H295R human adrenocortical cells by binding to the receptor, Mol. Cell Biol. 32 (21) (2012) 4419–4431.
[25] F. Arenas, F. Castro, S. Nuñez, G. Gay, C. Garcia-Ruiz, J.C. Fernandez-Checa, STARD1 and NPC1 expression as pathological markers associated with astrogliosis in post-morten brains from patients with Alzheimer's disease and Down syndrome 12 (2020) 571–592.
[26] Y. Lange, Y. Ye, M. Rigney, T. Steck, Cholesterol movement in Niemann-Pick type C cells and in cells treated with amphiphiles, J. Biol. Chem. 275 (2000) 17468–17475.
[27] L. Liscum, J.R. Faust, The intracellular transport of low density lipoprotein-derived cholesterol is inhibited in Chinese hamster ovary cells cultured with 3-beta-[2-(diethylamino)ethoxy]androst-5-en-17-one, J. Biol. Chem. 264 (1989) 11796–11806.
[28] S. Lucken-Ardjomande, S. Montessuit, J.C. Martinou, Bax activation and stress-induced apoptosis delayed by the accumulation of cholesterol in mitochoondrial membranes, Cell Death Differ. 15 (2007) 484–493.
[29] A. Fernandez, et al., ASMase is required for chronic alcohol induced hepatic endoplasmic reticulum stress and mitochondrial cholesterol loading, J. Hepatol. 59 (4) (2013) 805–813.
[30] A. Klein, et al., Lack of activation of the unfolded protein response in mouse and cellular models of Niemann-Pick type C disease, Neurodegener. Dis. 8 (3) (2011) 124–128.
[31] N. Mizutani, et al., Increased acid ceramidase expression depends on upregulation of androgen dependent deubiquitinases, USP2, in a human prostate cancer cell line, LNCaP, J. Biochem. 158 (4) (2015) 309–319.
[32] S.R. King, H.A. LaVoie, Gonadal transactivation of STARD1, CYP11A1 and HSD3B, Front. Biosci. (Online) 17 (2012) 824–846.
[33] J.E. Vance, Lipid imbalance in the neurological disorder, Niemann-Pick C disease, FEBS Lett. 580 (23) (2006 Oct 9) 5518–5524.
[34] C. Xie, S.D. Turley, J.M. Dietschy, Cholesterol accumulation in tissues of the Niemann-pick type C mouse is determined by the rate of lipoprotein-cholesterol uptake through the coated-pit pathway in each organ, Proc. Natl. Acad. Sci. U.S.A. 96 (21) (1999) 11992–11997. Oct 12.
[35] S. Takikita, et al., Perturbed myelination process of premyelinating oligodendrocyte in Niemann-Pick type C mouse, J. Neuropathol. Exp. Neurol. 63 (6) (2004) 660–673. Jun.
[36] C. Xie, et al., Cholesterol is sequestered in the brains of mice with Niemann-Pick type C disease but turnover is increased, J. Neuropathol. Exp. Neurol. 59 (12) (2000) 1106–1117. Dec;59.
[37] F.M. Platt, B. Boland, A.C. van der Spoel, The cell biology of disease: lysosomal storage disorders: the cellular impact of lysosomal dysfunction, J. Cell Biol. 199 (5) (2012) 723–734.
[38] L.D. Griffin, W. Gong, L. Verot, S.H. Mellon, Niemann-Pick type C disease involves disrupted neurosteroidogenesis and responds to allopregnanolone, Nat. Med. 10 (7) (2004) 704–711.
[39] E. Fayard, J. Auwerx, K. Schoonjans, LRH-1: an orphan nuclear receptor involved in development, metabolism and steroidogenesis, Trends Cell Biol. 14 (5) (2004 May) 250–260.
[40] B.P. Schimmer, J. Tsao, M. Cordova, S. Mostafavi, Q. Morris, J.O. Scheys, Contributions of steroidogenic factor 1 to the transcription landscape of Y1 mouse adrenocortical tumor cells, Mol. Cell. Endocrinol. 336 (2011) 85–91.
[41] J.W. Kim, N. Peng, W.E. Rainey, B.R. Carr, G.R. Attia, Liver receptor homolog-1 regulates the expression of steroidogenic acute regulatory protein in human granulosa cells, J. Clin. Endocrinol. Metab. 89 (2004) 3042–3047.
[42] N.C. Lucki, et al., Acid ceramidase (ASAH1) is a global regulator of steroidogenic capacity and adrenocortical gene expression, Mol. Endocrinol. 26 (2) (2012 Feb) 228–243, https://doi.org/10.1210/me.2011-1150.
[43] R. Duggavathi, et al., Liver receptor homolog 1 is essential for ovulation, Genes Dev. 22 (2008) 1871–1876.
[44] R. Sirianni, et al., Liver receptor homologue-1 is expressed in human steroidogenic tissues and activates transcription of genes encoding steroidogenic enzymes, J. Endocrinol. 174 (2002) R13–R17.
[45] O.B. Davis, et al., NPC1-mTORC1 signaling couples cholesterol sensing to organelle homeostasis and is a targetable pathway in Niemann-Pick type C, Dev. Cell 56 (2021) 260–276.
[46] Lloyd-Evans, et al., Niemann-Pick disease type C1 is a sphingosine storage disease that causes deregulation of lysosomal calcium, Nat. Med. 114 (2008) 1247–1255.
[47] J. Newton, et al., Targeting defective sphingosine kinase 1 in Niemann-Pick type C disease with an activator mitigates cholesterol accumulation, J Biol Chem May 8 (2020) papers in press.
[48] K. Kwiatkowska, et al., Visualization of cholesterol deposits in lysosomes of Niemann-Pick type C fibroblasts using recombinant perfringolysin O, Orphanet J. Rare Dis. 9 (1) (2014) 64, https://doi.org/10.1186/2750-1172-9-64.
[49] A. Baulies, et al., Lysosomal cholesterol accumulation sensitizes to acetaminophen hepatoxicity by impairing mitophagy, Sci. Rep. 5 (2015) 18017.